Institute of Physics Publishing Journal of Physics: Conference Series **54** (2006) 176–182
doi:10.1088/1742-6596/54/1/030 Galaxy Center Workshop 2006

A mid-infrared survey of the inner 2 x 1.5 degrees of the Galaxy with Spitzer/IRAC

S. Stolovy[1], S. Ramirez[2], R. G. Arendt[3], A. Cotera[4], F. Yusef-Zadeh[5], C. Law[5], D. Gezari[6], K. Sellgren[7], J. Karr[8], H. Moseley[6] and H. A. Smith[9]

[1] Spitzer Science Center, California Institute of Technology, Pasadena, CA 91125
[2] IPAC/Caltech
[3] SSAI/GSFC
[4] SETI Institute
[5] Northwestern Univ.
[6] GSFC
[7] Ohio State Univ.
[8] Academia Sinica
[9] CfA

E-mail: stolovy@ipac.caltech.edu

Abstract. We present a survey of Spitzer Space Telescope/IRAC observations of the central 2 x 1.5 degrees (265x200 pc) of the Galaxy at 3-8μm. These data represent the highest spatial resolution and sensitivity large-scale map made to date of the Galactic Center (GC) at mid-infrared wavelengths. The IRAC data provide a census of the optically obscured stellar sources as well as a detailed map of the highly filamentary structure in the interstellar medium. The diffuse emission is dominated by PAH emission from small grains in star-forming regions. Dark clouds displaying a large variety of sizes and morphologies are imaged, many of which remain opaque at IRAC wavelengths. Using a multiwavelength comparison, we determine which objects are likely to be in the foreground and which are located at the GC. We find no counterparts at IRAC wavelengths to the unique system of linear, nonthermal radio filaments present at the GC.

1. Motivation

The IRAC instrument aboard the Spitzer Space Telescope is extremely well-suited to mapping out large areas of the sky efficiently while penetrating the interstellar dust that makes observing regions such as the GC impossible at optical wavelengths. We chose to map the central 2 x 1.5 degrees of the Galaxy in order to cover much of the Central Molecular Zone of the Galaxy, with a scientific emphasis on studying objects that are located at the GC. At a galactocentric distance of 7.6 kpc ([1]), our survey covers the inner $\sim$ 265 x 200 pc of the Galaxy. IRAC obtains simultaneous 5.2'x5.2' images at wavelengths centered at 3.6, 4.5, 5.8 and 8.0 μm, which we also refer to as Channels (Ch)1-4, respectively. Each of the 4 cameras consists of an array of 256x256 pixels with 1.22"x1.22" pixels. Ch 1, 2, and 3 are undersampled, and Ch 4 is nearly Nyquist sampled (at 8 μm, λ/2D is 0.97$''$). We consider the spatial resolution of the entire survey to be on order 2$''$ (0.07pc at the GC).

IRAC observations provide a stellar census between the Sun and GC as well as a map of the diffuse PAH emission seen near star forming regions. Previous near-IR surveys such as 2MASS and DENIS, although providing a basis for resolving and understanding the stellar population

© 2006 IOP Publishing Ltd

toward the GC, are limited in that the longest wavelength of 2.2 μm is insufficient to observe the most obscured regions, and longer wavelengths are needed to measure IR excesses. The MSX survey of the Galactic Plane imaged the diffuse dust emission from PAH molecules at 8μm and from larger dust grains (out to $\sim$ 21μm) but lacked the spatial resolution to properly resolve individual stars; at 8 μm, the MSX resolution is 18$''$. The infrared dark clouds discovered with MSX ([2]) are now imaged with 10 times better spatial resolution with the IRAC data. The GC was also observed with ISOCAM as part of a galactic plane survey called ISOGAL at 7 and 15μm with 3$''$ pixels ([3]). These data, especially the 15 μm observations, will provide a useful complement to this dataset. However, the ISOGAL survey did not observe the central regions of high interest such as Sgr A and the Arched Filaments due to saturation.

2. Observations and Data Reduction

The entire region was surveyed using what is referred to as the '2 second' exposure time using the full (5.2'x5.2') array, but which represents an actual integration time of only 1.2 second per pixel on the sky. Five 'medium' dithers were taken for each pointing in order to correct for bad pixels, scattered light, and latent images as well as to better sample the point spread function. Therefore the total average integration time on the for the survey is 6 seconds in each channel. At this depth, we are confusion limited everywhere except toward dark clouds that are so opaque that they are dark even at IRAC wavelengths.

We performed additional processing on the pipeline version S13.2 BCD (basic calibrated data) pipeline products in order to correct for various instrumental effects, including: corrections for scattered light, latent images, column pulldown (Ch1 and 2) and banding (Ch 4). The total number of full-array BCD's obtained in each IRAC array was 2895, organized into 12 AORs (Astronomical Observation Requests). The brightest regions of the survey were observed last to minimize the effects of latent images. The full-array map was obtained between March 29 and March 31, 2005. The fields of view projected on the sky are nearly identical for IRAC Channels 1 and 3 and Channels 2 and 4, respectively, but those pairs of channels are offset on the sky by about 400$''$. We mapped a slightly larger region than 2 x 1.5 degrees in order to get full coverage in all 4 channels. In this paper, however, we crop our mosaics slightly to trim the jagged edges; Fig. 1 displays an area covering 2 x 1.4 degrees.

We used mopex (available from ssc.spitzer.caltech.edu/postbcd/download-mopex.html) to create mosaics resampled to 1.0$''$ pixels and to extract point sources. The resultant mosaics represent a significant improvement over available SSC pipeline products. Our mosaics exhibit seamless continuity in the background level. Some detector artifacts remain, however; the most obvious one is the "bandwidth effect" which causes extra 'sources' to appear 4 pixels away (and in some cases 8 pixels away) from very bright sources due to an electronic effect of the 4 readout channels in Ch3 and Ch4.

Although only a tiny fraction of the area covered was saturated, we aimed to produce a high quality mosaic across the entire region. Thus, we obtained data in IRAC's subarray mode for regions that were saturated in the 2 second exposures 6 months after the main survey. In subarray mode, a small section of the array is read out (32x32 pixels = 40"x40"), and we used the shortest exposure time available of 0.02 sec. Sixteen targeted objects (including the brightest regions in the survey, Sgr A West and the 'IR Quintuplet' cluster (see Fig. 2) were observed in subarray mode on Sept. 15, 2005. The entire survey, including both full and subarray exposures, was completed in less than 16 hours of telescope time. The subarray data were substituted for the saturated full array data in the analysis presented here.

These GC observations will be incorporated into the larger GLIMPSEII survey (PI: Churchwell, Program ID= 20201), which maps the Galactic Plane interior to $\pm$ 10 degrees of Galactic latitude. For the longitude range of $\pm$ 2 degrees, GLIMPSEII extends the map out to $\pm$ 2 degrees of latitude to better map the bulge. The GLIMPSEII team will make data products

available to the public including BCD's, mosaics and point source catalogs, all of which will be available through the Spitzer Science Center archive. The GLIMPSEII products will differ from our independently derived version. High resolution jpgs (each 7002x5050 pixels) of both the 4-color composite and the 8μm-only image are are available for download from the press release archive at ssc.spitzer.caltech.edu. We encourage readers to access these images; the small format available here cannot convey the rich details that are present. Due to page limits, we show only the Ch1 and Ch4 mosaics; Ch2 looks very much like Ch1 and is dominated by point sources, and Ch3 has both point sources and PAH emission that is weaker by about a factor of 3 compared to the Ch4 mosaic.

3. Properties of Point Sources

Point source extraction and properties of the point sources will be discussed in more detail elsewhere (Ramirez et al. in prep., Cotera et al., these proceedings), but we provide a summary here. We performed both point response function (PRF) fitting and aperture photometry on the BCD's and compared the two methods to make our final catalog. We chose a small aperture to avoid confusion and applied an aperture correction for the aperture flux. We found that the aperture fluxes were systematically lower than the PRF fluxes and we adjusted the aperture fluxes such that the median ratio of the two sets was 1. We produced source-subtracted images to assess the effectiveness of the extraction. We found that the PRF fitting occasionally failed and predicted a flux that was much too high. For the cases where the PRF/aperture flux ratio exceeded 1.3, we adopted the adjusted aperture value. The source-subtracted residual images show even fainter sources but we did not attempt to extract them. Additionally, the brighter sources close to saturation are in the nonlinear regime and therefore do not match the PRF. We have significantly improved our point source extraction techniques since the conference presentation and we present the newest results here.

The total number of sources detected at a level of 3σ or above in each channel was: 893417, 819914, 535809, and 385926 for Channels 1, 2, 3, and 4, resp. The number of sources common within a 1$''$ radius all 4 bands was 284,676. The extraction thus far has been done only on the full array data. We intend to update the catalog with extractions from the subarray data in the future. We have bandmerged our IRAC catalog with the 2MASS catalog, which has comparable spatial resolution, and we are in the process of analyzing the SEDs of the sources. The vast majority of point sources are red giants and AGB stars.

Figure 3 shows the flux distribution for each of the channels for the entire survey. We adopt zero magnitude definitions in the Spitzer Observer's Manual of 280.9, 179.7, 115.0, 64.13 Jy for Ch. 1, 2, 3, and 4, resp. In a survey with relatively uniform background, one might be able to use a diagram such as Figure 3 to estimate the confusion limit near the peak of the counts before the dramatic plunge at the faint end. However, there is no single number that characterizes the confusion in this survey due to the large diversity of background levels against which these sources are extracted. To illustrate this point, Fig. 4 shows the flux distributions in Ch. 1 toward diverse regions with equal 4'x4' areas: 1) in the plane in a region of high surface brightness (dash-dot) between Sgr A and the Arches, 2) away from the plane but also away from dark clouds (thick solid line), 3) towards Sgr B2, a GC dark cloud in the plane (dotted line) and 4) towards a dark foreground cloud (thin solid line). The confusion limit in region 1 is about 2 magnitudes brighter than the others (roughly 11.5 vs 13.5), and there are also significantly more bright sources detected in region 1. It's also clear that the foreground dark cloud blocks many of the faint sources behind it that are detected in 2) and 3). Regions 2 and 3 have nearly identical distributions; implications for Galactic structure are that we may be detecting faint stars beyond the distance of the GC (or at least beyond the distance to Sgr B2) when observing away from the plane. Galactic coordinates are given in the caption.

4. Properties of the Diffuse Emission

PAH Emission The diffuse, highly filamentary structure seen in the IRAC mosaics are dominated by emission from very small grains known as polycyclic aromatic hydrocarbons (PAH's). The PAH's are excited by UV photons and emit in infrared bands centered on 3.3, 6.2, 7.7, 8.6, and 11.3 μm. PAH's are observed in Ch 1, 3, and 4, with the 7.7 μm line in Ch 4 being the dominant band. The PAH emission emanates from photodissociation regions (PDRs) and is generally indicative of star forming regions. For GC objects, the PDR and ionized HII regions often appear in projection to be coincident. The PAH's are transiently heated; since they do not achieve thermal equilibrium, dust temperatures cannot be derived by comparing the IRAC bands. In fact, the ratios of the mosaics (for instance, Ch4/Ch3) show remarkable uniformity across the entire region. This supports the idea, without having to do extensive spectroscopy, that the diffuse emission in the IRAC data is dominated by PAH emission. The line strengths of the PAH bands are nearly constant over several orders of magnitude of radiation field strength ([4]). Very weak extended emission is seen in some regions in Ch1 (PAH 3.3 μm band) and Ch2 (Brα , H_2, and CO lines are in this band). A few compact star forming regions, such as the 'H1-8' regions near the base of the thermal Arched Filaments have an excess in Ch4/Ch3 . We interpret the excess as arising from thermal emission from larger dust grains in exceptionally high radiation fields near regions of massive star formation.

Dark Clouds and Extinction Dark clouds are imaged with exquisite detail, and display a large variety of morphologies. Long, stringy, filamentary structures are often seen. The darkest clouds in our images must be located in the foreground, because they block the light from the background red giants and AGBs seen elsewhere. In addition, most of the dark clouds are physically associated with (adjacent to) clouds with bright PAH emission. The presumption is that star formation is progressing through a cloud. Sgr B2 (center left in Fig. 1) is known to be located near the GC; although we do detect several compact diffuse objects coincident with radio emission, it is remains highly obscured. A comparison with images from the SHASSA survey ([5]) reveals that many of the diffuse objects displaced a few tenths of a degree from the Galactic plane have Hα emission associated with them, and in many cases the PDR and ionized regions are displace from each other rather than superposed. Wherever Hα is detected, the extinction must be less than a few visual magnitudes, which places them in the foreground. In contrast to filamentary dark clouds, very compact dark globules are observed in many places in absorption against the bright emission in the plane; some of these globules are only 5$''$ in size (less than 0.2 pc if located close to the GC); the size scales are consistent with what has been reported from near-IR observations ([6]). An extinction law was derived by [7] towards diverse regions in the Galactic plane that is nearly constant in the IRAC bands. We estimate that we are sensitive to sources seen through visual extinctions of Av$\sim$ 40-50, and we confirm that there is little "reddening" in the IRAC bands.

The Sickle, Pistol, and Quintuplet As an example of the detail and dynamic range present in the larger mosaics, Figure 2 shows 3.6'x3.6' subimages of Ch1 and Ch4 images of the objects known as the Sickle, Pistol and Quintuplet. With the incorporation of subarray data, the IR Quintuplet is unsaturated. Our data reveal that the Sickle is resolved into finger-like structures, likely photoevaporated by the hot stars in the Quintuplet (see Cotera et al., these proceedings.) The Pistol star is clearly observed and is in the center of a bubble-like nebula. The Pistol nebula is observed *only* in Ch4; the lack of Ch3 emission is consistent with the diffuse emission being dominated by [ArII] emission, which was observed with ISO spectroscopy (Moneti et al. in prep.).

Large-scale filamentary structures The GC Lobe is a loop-like structure that spans the central degree of the Galaxy in the radio continuum as well as at mid-infrared wavelengths. It was first observed in the infrared by MSX ([8]) and often is interpreted as a mass outflow from the GC region. The remarkable twisted pair of filaments seen on the eastern side of the GC lobe

was recently observed with Spitzer's MIPS-24 μm instrument and was dubbed the Double Helix Nebula (DHN) by [9]. The DHN is also observed in our Ch3 and Ch4 images, as is the western and brighter side of the GC lobe. The Ch4 image of the DHN is shown in Fig. 5; we note that the southern end is the most collimated part but it abruptly dissipates southward and does not connect in any obvious way to IR-emitting objects located at the GC. The western lobe (to the upper right of the Ch4 mosaic in Fig. 1) shows a more extensive "feathery" morphology but shares similarities with the DHN in that both have undulations with similar spatial frequencies. However, the well-defined helical morphology is seen only in the DHN. The Ch4/Ch3 color ratio implies that both sides of the GC Lobe are dominated by PAH emission in the IRAC data. The UV sources for the PAH emission may simply be the local radiation field, as the PAH emission can be excited by relatively cool stars.

Law (PhD thesis) obtained observations of the Lobe region with the GBT and VLA and found evidence in that the GC Lobe has a single origin and is located in the GC region. In radio continuum emission, the two sides of the Lobe are parallel and have a similar, distinctive curve. A comparison of radio and IR data imply that the GC Lobe exhibits concentric shells of gas observed (from interior to exterior) in: radio recombination lines (at zero velocity), radio continuum, and at the outer edge, the PAH emission. The east and west sides are not symmetrically displaced in longitude from Sgr A*, but they do appear to coincide with the longitudinal positions of the brightest nonthermal filaments; near the Arches to the east and the Sgr C filament to the west. Thus, they may be related to interactions of the relativistic electrons and the ISM rather than a process originating in the central few parsecs.

Another large-scale arc-like structure that is about 0.4 degree long is seen in the southwestern part of the image and can be seen to the lower right in the Ch4 image in Fig 1. It has a more diffuse nature than the GC Lobe and has no radio emission associated with it to date. It appears to originate, at least in projection, from a little-studied HII region near (l,b)=(359.59, -0.30) that also has a dark cloud associated with it and is likely a foreground object. It is possible that this large feature is also located in the foreground. A star forming region to the northeast (upper left) near (l,b)=(0.67,0.66) is clearly a foreground object with Hα filling in the PAH hourglass structure; the HII region is likely ionized by a known foreground B star.

Comparison with Radio Continuum Data The GC is a strong source of both thermal and nonthermal radio emission, which are distinguished by the spectral index at radio wavelengths. The thermal emission arises from the ionized gas as typically seen in star forming regions. The nonthermal emission is observed towards a number of sources, including Sgr A*, supernova remnants (SNRs) and, most remarkably, the complex and mysterious system of long, linear, filaments spanning in some cases tens of parsecs, the brightest of which are perpendicular to the Galactic plane ([10]).

The Ch4 data have a much higher signal/noise in the diffuse emission than the existing radio data. Nearly every known *thermal* region has a Ch 4 counterpart with the exception of Sgr B2, which is so heavily extincted that very little emission is seen even at 8 μm. Filamentary structures without clear radio counterparts are seen in Ch4 (Fig. 6) arching nearly perpendicular to the Galactic plane between Sgr A and the Arched Filaments. In contrast, there are NO IRAC diffuse structures that are spatially coincident with *nonthermal* radio emission. This is not surprising, as the PAH emission and the nonthermal radio emission arise from different environments. We constrain the spectral index in the linear filaments to be steeper than -0.6. Fig. 6 illustrates that the curved thermal arched filaments roughly parallel to the plane do show a close correlation between radio continuum emission and Ch4 emission. Known SNRs from radio data (e.g. Sgr A East, Sgr D SNR) are not detected in our survey; shocked H_2 emission (in Ch2) is likely too weak relative to the high background to be detected.

The Central Few Parsecs Sgr A* itself is too faint to detect in the IRAC data, and the central region is highly confused due to the large pixel size. The central "minispiral" and inner

edge of the circumnuclear disk are clearly imaged in Ch4 and we note that IRS8 is exceptionally bright. Thermal HII regions around the edge of the Sgr A East remnant are observed, along with embedded point sources. The 50km/s and 20km/s clouds are seen in extinction.

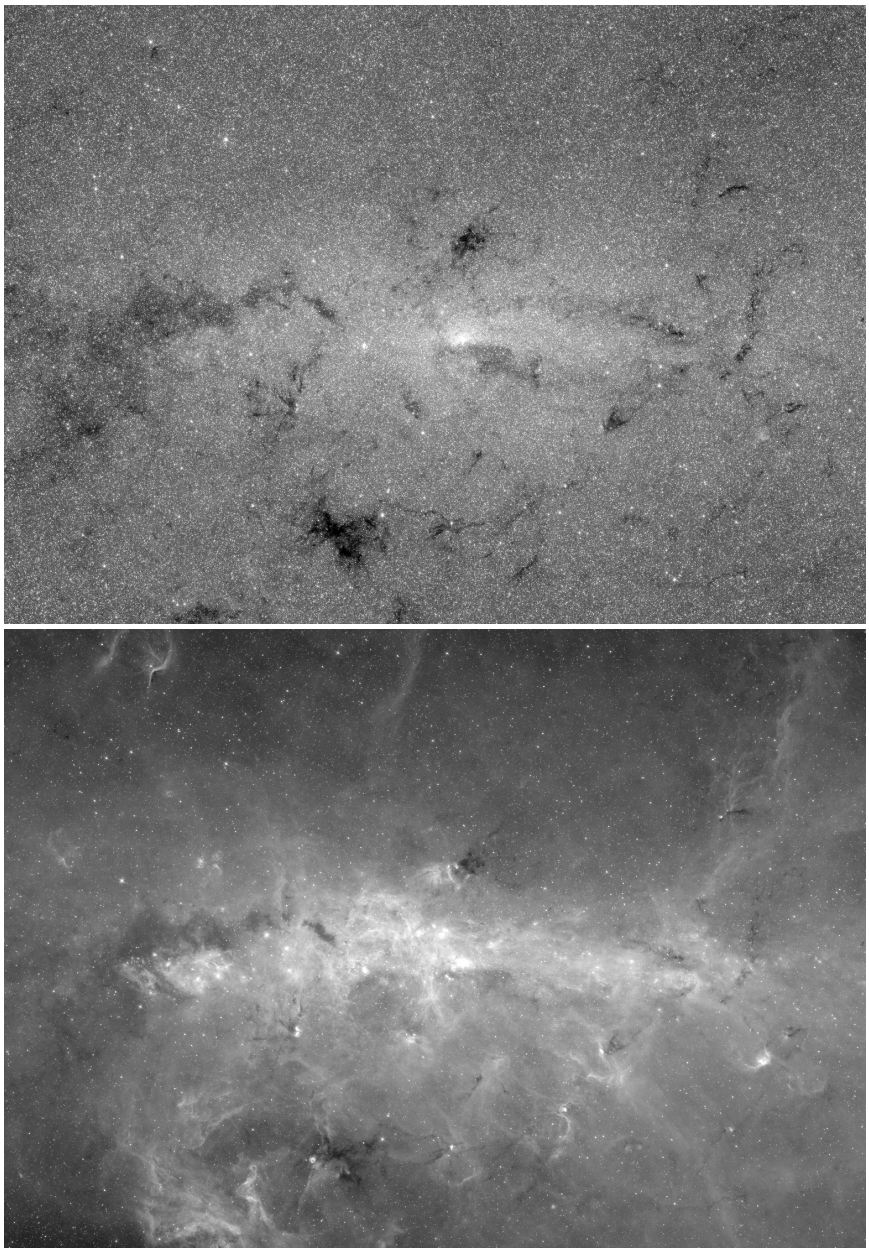

Figure 1. Mosaics of Ch1 (3.6μm, top) and Ch4 (8.0μm, bottom), in logarithmic grayscale. Galactic east is to the left and these images span l=$\pm$ 1 degree and b=$\pm$ 0.7 degree. The dynamic range in each image spans $\sim$ 5 orders of magnitude.

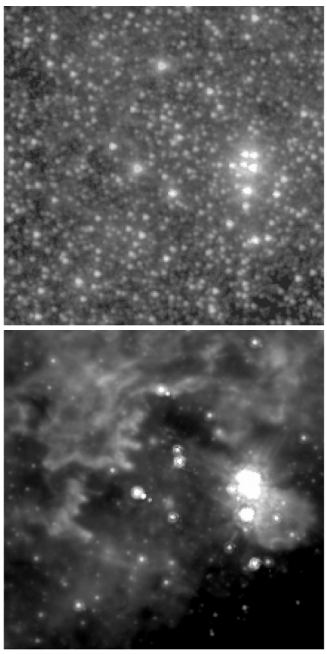

Figure 2. Quintuplet, Pistol, and Sickle region in Ch1 (top) and Ch4 (bottom), combining the full array data with subarray data taken 6 months later. The area shown is 3.6' on a side with Galactic east to the left.

References

[1] Eisenhauer, F. et al. 2005 *ApJ* **628**, 246
[2] Egan, M.P. et al. 1998, *ApJ* **494** 199

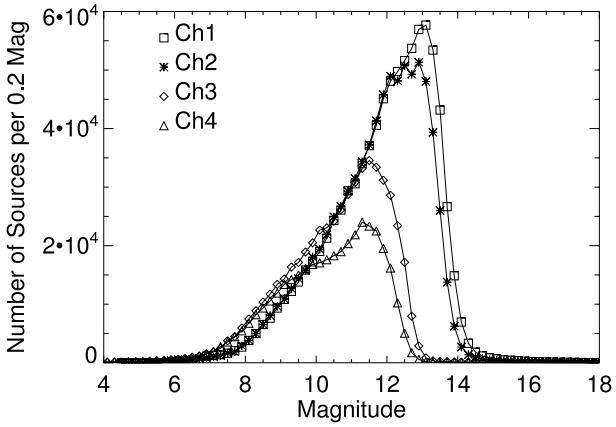

Figure 3. Histogram of point source detections for Ch1 (3.6μm, squares), Ch2 (4.5μm, asterisks), Ch3 (5.8μm, diamonds) and Ch4 (8.0μm, triangles) for the entire survey.

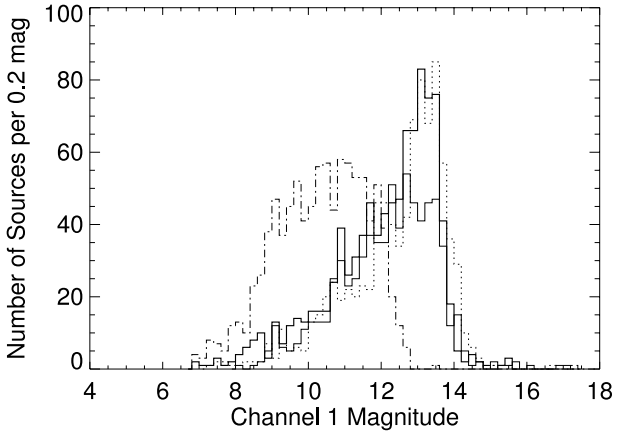

Figure 4. Histogram of Ch1 fluxes in a 4'x4' aperture towards the following regions in (l,b): 1) dash-dot: (0.06, -0.05) (2) thick solid: (359.93,0.64) 3) dotted: (0.63,0.00); 4) thin solid: (359.93,0.17). The total number of sources detected in each region are: 967, 966, 884, and 733 for regions 1-4, resp.

Figure 5. Double Helix Nebula at 8μm, with the fainter point sources removed for clarity. This is the eastern part of the Galactic Center Lobe.

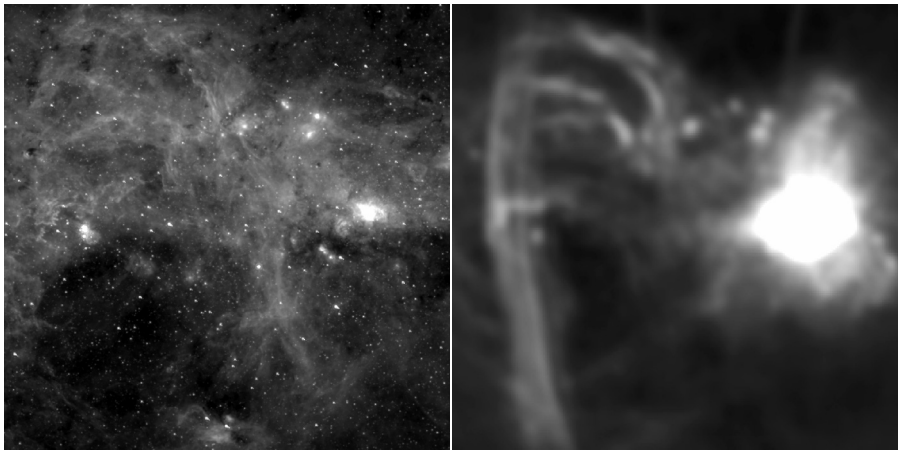

Figure 6. Sgr A/Arched Filaments region in Ch4 (left) and 20cm radio emission. The linear, nonthermal filaments are not observed with IRAC, but Ch4 counterparts to thermal objects are seen. The images are 20.5′ (45.3 pc) on a side with Galactic east to the left and centered at (l,b)=(0.057,-0.060). The radio image (from [10]) has 30″ resolution.

[3] Omont, A. et al. 2003 *A&A* **403** 975
[4] Li, A. & Draine, B. 2001*ApJ* **554** 778
[5] Guastaud, J. et al. 2001 *PASP* **113** 1326
[6] Gosling, A., Blundell, K. and Bandyopadhyay, R. 2006 *ApJ* **640**, 171
[7] Indebetouw, R. et al. 2005 *ApJ* **619** 931
[8] Bland-Hawthorn & Cohen 2003 *ApJ* **582** 246
[9] Morris, M., Uchida, K. and Tuan, D. 2006 *Nature* **440** 308
[10] Yusef-Zadeh, F., Hewitt, J. W., & Cotton, W., 2004 *ApJS* **155** 421